THE JOURNAL OF PHYSICAL CHEMISTRY C

Article

Cite This: J. Phys. Chem. C 2017, 121, 27766−27773

pubs.acs.org/JPCC

Role of Valley Anisotropy in Optical Absorption of Monodisperse PbS Nanocrystals

Alexander N. Poddubny,[†,‡] Valentina M. Litvyak,[§] Mikhail O. Nestoklon,[†] Roman V. Cherbunin,*[,§] Valerii V. Golubkov,[∥] Petr A. Onushchenko,[∥] Anastasiya N. Babkina,[‡] Alexei A. Onushchenko,[⊥] and Serguei V. Goupalov*[,#,†]

[†]Ioffe Institute, St. Petersburg 194021, Russia

[‡]ITMO University, St. Petersburg 199034, Russia

[§]St. Petersburg State University, St. Petersburg 198504, Russia

[∥]Institute of Silicate Chemistry of RAS, St. Petersburg 199034, Russia

[⊥]NITIOM SI Vavilov State Opt Inst, 36-1 Ul Babushkina, St. Petersburg 192171, Russia

[#]Department of Physics, Jackson State University, Jackson, Mississippi 39217, United States

ABSTRACT: We study light absorption by nearly monodisperse PbS nanocrystals grown in a glass matrix. The absorption spectra demonstrate a well-resolved structure at energies above the first absorption peak. The absorption cross sections are calculated with an empirical tight-binding model accounting for the quantum confinement, the band anisotropy, and valley splittings. Absorption spectra measured at 4 K quantitatively agree with the atomistic calculations. This allows us to unambiguously ascribe the much-debated second absorption peak to the p−p optical transition and directly measure the splitting of excited p states.

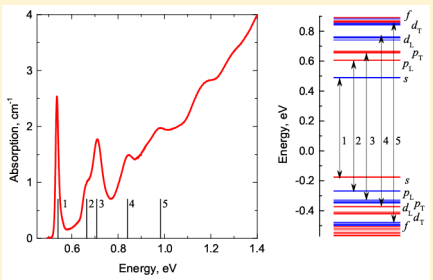

INTRODUCTION

Lead sulfide (PbS) nanocrystals are highly promising for light-emitting devices,[1−4] photodetectors,[5,6] and photovoltaic[7−11] applications. Tremendous progress has been made in the synthesis of colloidal PbS quantum dots over the past decade.[11−15] State-of-the-art technologies enable fine on-demand engineering of optical spectra by surface chemistry[16−18] and even self-organized growth of 3D nanocrystal superlattices.[19] Nevertheless, the connection between the energy spectra and optical properties remains a subject of ongoing debate. The reason is that lead chalcogenides (PbS, PbSe, PbTe) have a complex energy band structure.[20] The extrema of both conduction and valence bands are located at the four L points of the Brillouin zone forming four inequivalent anisotropic valleys. This leads to a high degeneracy of the energy spectrum in bulk materials. This valley degeneracy is lifted in nanocrystals due to the surface scattering. The resulting energy spectra of lead chalgodenide nanocrystals become quite intricate, especially for the excited states. The widely used 4 × 4 effective mass model for nanocrystals, put forward by Kang and Wise in 1997,[21] neglects both the intervalley mixing and the anisotropy of the effective masses, known to be large: $m_{e,l} = 0.105m_0$, $m_{e,t} = 0.080m_0$, $m_{h,l} = 0.105m_0$, and $m_{h,t} = 0.075m_0$ for PbS (m_0 is the free electron mass, $m_{e(h),\ l(t)}$ is the electron (hole) band-edge longitudinal (transverse) effective mass).[22] Analysis of the optical absorption spectra shows that the Kang and Wise model adequately describes the nanocrystal size dependence of the fundamental energy gap, corresponding to the lowest-energy optical transition, but cannot explain the origin of the second absorption peak. Namely, the observed energy of the second absorption peak is very close to the energy of the $s_{e(h)}$−$p_{h(e)}$ transition following from the Kang and Wise model (we use the orbital momentum notation s, p, and d to describe the symmetry of the envelope wave function[23]). However, this transition is forbidden in the effective mass approximation[21] because of the parity selection rules. Two explanations of the apparent discrepancy have been proposed. The first explanation argues that the anisotropy effects[24−26] and intervalley coupling[27] split and shift the spectrum of Kang and Wise,[21] so that the observed second spectral line in fact corresponds to the allowed (split) p_e−p_h transitions. According to the second line of arguments,[23,28−30] the parity selection rules are relaxed in nanocrystals as compared with the bulk, so the second observed transition is in fact the s−p one. For PbSe nanocrystals, the results of power-dependent pump−probe spectroscopy[31] favor the first, p−p explanation, which is also consistent with the results of the scanning tunneling spectroscopy of the density of states.[32] Trinh et al.[31] have studied the probe absorption at the second transition after pumping in resonance with the first one and failed to observe the bleaching effect, which rules out the contribution of s levels to the second

Received: October 31, 2017
Revised: November 20, 2017
Published: November 20, 2017

DOI: 10.1021/acs.jpcc.7b10778
J. Phys. Chem. C 2017, 121, 27766−27773

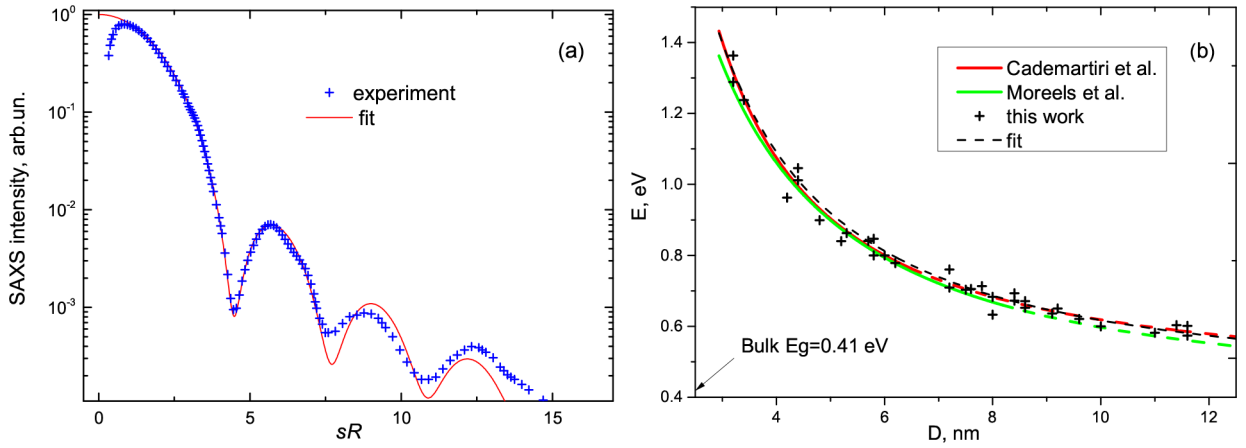

Figure 1. (a) SAXS intensity as a function of scattering angle measured on PbS nanocrystals in glass. Blue crosses are experimental data for a sample with mean nanocrystal diameter D = 8 nm, and red line is fitting by eq 2 of the Experimental Methods. (b) Dependence of the energy of first optical transition on quantum dot diameter measured by SAXS (black crosses). Comparison with fitting from other works.[13,14]

transition. On the contrary, the experiments by Nootz et al.[33] with PbS and PbSe nanocrystals show one-photon and two-photon absorption at the same energy, thus hinting toward the relaxation of the parity selection rules and the s−p origin of the second transition. For PbS nanocrystals, the question about the origin of the second transition is not settled at least as of 2013.[34] Diaconescu et al.[34] have visualized the nanocrystal density of states by means of the scanning tunneling spectroscopy and compared it with the one-photon absorption data of Nootz et al.;[33] their analysis favors the parity breaking explanation for the second transition. Recently, the detailed experimental study of the size-dependent absorption spectra of PbS nanocrystals in glass has been performed.[35] The high-energy peaks in the absorption spectra were attributed to defect states at the nanocrystal interface.

The existence and the long history of the debate on the origin of the second transition in PbS nanocrystals could be explained by several reasons.

On the experimental side, the optical absorption of colloidal samples is inhomogeneously broadened due to the size dispersion, which was ∼10% in early studies,[12] 6−10% for the samples of Cademartiri et al.,[13] and has dropped below 5% only recently.[15] PbS nanocrystals grown in glass matrices exhibit a large scatter of this parameter from 15−20%[36] to 5−7%[37] depending on the realized stage of the supersaturated solid solution decomposition. Only the latter samples demonstrate well-resolved absorption spectra allowing to observe the second optical transition.

On the theory side, the works in anisotropic $\boldsymbol{k}\cdot\boldsymbol{p}$ approximation[24,25] have neglected the intervalley splitting and did not provide direct comparison of calculated and experimental spectra. The more elaborate empirical tight-binding models were put forward only for PbSe quantum dots[28] and did not account for the effective mass anisotropy of PbSe.[28] The semiempirical pseudopotential calculations[27] have also focused only on PbSe.

The ab initio calculation of bulk energy structure of lead chalcogenides is difficult due to their narrow gap in L point and strong spin−orbit interaction on semicore Pb d orbitals. In particular, the standard density functional theory based on either the local-density approximation (LDA) or the generalized gradient approximation (GGA) fail to reproduce even the correct order of the bands near the band gap. This can be overcome by using the hybrid functionals[38] or the GW approach,[38,39] which allows one to obtain a good agreement with the experimental data. However, because of computational complexity these approaches can be hardly applied to the calculations of the nanostructures. The attempts to extract electron and hole effective masses directly from the ab initio calculations to reach a reasonable agreement with experimental data are also still challenging.[40]

Considerable progress was made in our 2012 work,[41] where the bulk dispersion[39] and the experimental effective masses[22] were fitted to finally obtain the empirical $sp^3d^5s^*$ tight-binding approximation, suitable for large-scale calculations of lead chalcogedide nanostructures.

In this work we aim to clarify the origin of peaks in optical absorption spectra of PbS nanocrystals armed with high-quality samples and state-of-the-art atomistic calculation techniques. Namely, we consider nearly monodisperse PbS nanocrystals in glass with the size dispersion of ∼5% on par with the best colloidal quantum dots.[15] The experiment is corroborated by empirical tight-binding calculations based on our model[41] that explicitly accounts for the three main effects[27] in the energy spectra: the quantum confinement, the band anisotropy, and the valley splittings. This enables us to undertake a quantitative comparison between the measured and the calculated absorption spectra. The resolution of experimental absorption spectra is high enough to directly see the splitting of p−p transitions, caused by the valley anisotropy, and unambiguously attribute the second and the third peaks in optical absorption spectra to the longitudinal and transverse p−p transitions, respectively.

RESULTS AND DISCUSSION

Monodisperse PbS Nanocrystals. Samples of PbS nanocrystals with varying mean diameters in the range $D \approx 4\div11$ nm were grown in glass matrices. The samples were characterized by means of the small-angle X-ray scattering (SAXS) technique. More details are given in the Experimental Methods. Both mean diameters and nanocrystal size dispersions were estimated from fits of the SAXS intensity dependence on the scattering angle. A typical SAXS pattern is given in Figure 1a. The nanocrystal size dispersion was on the order of 5% depending on the sample and reached as low as 4.5%. Next, the optical absorption spectra were measured for all

DOI: 10.1021/acs.jpcc.7b10778
J. Phys. Chem. C 2017, 121, 27766−27773

samples at 4, 77, and 300 K. Figure 1b summarizes the dependencies of the ground state optical transition energy on the mean nanocrystal diameter, obtained in our work and by other groups. As expected, the quantum confinement leads to the blue shift of the transition energy for smaller diameters.[42] Black crosses in Figure 1b correspond to our experimental measurements at T = 300 K. They can be well fitted by the empirical dependence $E = E_g + 4.06\ \text{eV}\cdot(1\ \text{nm}/D)^{1.3}$ (black dashed line). Red and green lines in Figure 1b show dependencies of the first optical transition energy on the quantum dot diameter measured by transmission electron microscopy (TEM).[13,14] Solid green and red lines correspond to the range of diameters in the experiments,[13,14] while dashed green and red lines are extrapolations beyond these regions. The literature data for colloidal quantum dots are in a good agreement with our results. Recent Rayleigh and Mandel'shtam-Brillouin scattering (RMBS) results obtained for glasses containing PbS nanocrystals[43] give an additional confirmation of the nanocrystal size assignment made by the SAXS measurements.

Having reproduced the well-known data for the first peak in optical absorption, we now proceed to the calculation of the interband absorption spectra, involving excited states of holes and electrons and their comparison with the experiment.

Anisotropy-Split Excited States Manifested in Optical Absorption. The absorption spectra have been calculated in the framework of our empirical $sp^3d^5s^*$ tight-binding model for PbS, developed and described in detail in our work.[41] The modeled nanocrystals had spherical shape: They were "carved out" from the bulk rocksalt structure by a sphere drawn around the center of the minimal lattice cube formed by Pb and S atoms, and the lattice strain was neglected. The optical matrix elements were evaluated in the diagonal approximation for the coordinate matrix element, that is, neglecting the intraatomic transitions.[44] Figure 2a shows the calculated energy dependence of the optical absorption cross section for the PbS nanocrystal of the diameter $D \approx 6.5$ nm. The calculated spectral lines were broadened by the Gaussians with the dispersion δ = 40 meV (thick black curves) and δ = 5 meV (thin red curves). This broadening phenomenologically accounts for the actual homogeneous and inhomogeneous broadening of the nanocrystal ensemble, inevitable in the experiment. For δ = 40 meV, one can resolve five broad optical absorption peaks in the range of photon energies $E \lesssim 1.4$ eV, as indicated at the top of Figure 2a. As will be shown later, the value of δ = 40 meV roughly corresponds to our experimental absorption spectra. The spectrum calculated for δ = 5 meV reveals that each of the peaks 3, 4, and 5 does not correspond to just a single optical transition but is contributed by several transitions with varying oscillator strengths and slightly different energies.

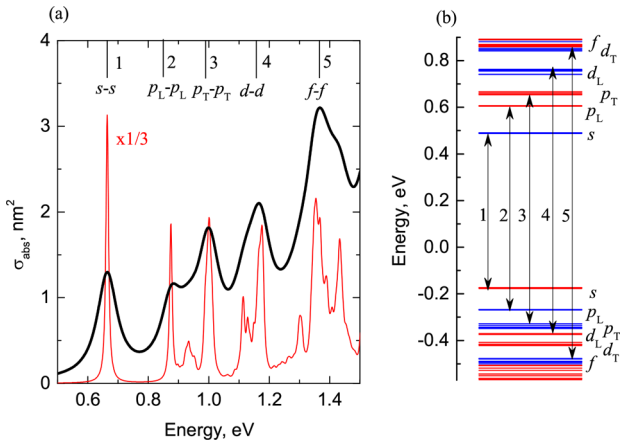

Figure 2. Calculated absorption (a) and energy (b) spectra for PbS nanocrystal with $D \approx 6.5$ nm. Thick black and thin red curves in panel a are calculated with homogeneous broadening δ = 40 and 5 meV, respectively. Major transitions 1−5 are indicated by vertical lines in panel a and arrows in panel b. Blue (red) lines in panel b correspond to odd (even) parity of the states.

To elucidate the origin of the optical transitions, we have plotted in Figure 2b the energy spectrum of the nanocrystals under study. Whereas, for the chosen geometry, the nanocrystals do not possess microscopic inversion centers, the analysis of the tight-binding wave function shows that parity can still be considered as a good quantum number. The transitions between the states of different parity have weak oscillator strengths and cannot be resolved in the absorption spectra. In Figure 2b we show by blue (red) lines the energies of the states, odd (even) with respect to the cation. This procedure allows one to separate the quantum confined states of electrons and holes into well-resolved multiplets and uncover the origin of the optical transitions. The ground states of electrons and holes are labeled in Figure 2b as s states. The transition 1 in Figure 2a is the s−s transition. The s states have two-fold degeneracy with respect to spin and also almost complete four-fold valley degeneracy, as the valley splitting cannot be resolved for $D \approx$ 6.5 nm on the scale of Figure 2b. The energy spectrum of excited states becomes more complex. There exist $3 \times 4 \times 2 =$ 24 excited p states of electrons and holes, differing by the orientation of the p orbital with respect to the L valley direction, by the valley number, and by the spin. The anisotropy of effective masses of PbS splits these states into 8 longitudinal states and 16 transverse ones. This splitting is well resolved in Figure 2b; the longitudinal states are lower in energy by ∼50 meV than the transverse ones. An analysis of the transition energies and oscillator strengths unambiguously indicates that the transition 2 in Figure 2a takes place between longitudinal p states of both holes and electrons (p_L−p_L). The transition 3 is the transition between transverse states (p_T−p_T). The transition between the states with different orbital momentum directions is also possible but has a low oscillator strength. It corresponds to the weak peak at about 0.95 eV in Figure 2a, which can be resolved for a small spectral broadening (red curve) but is washed out for realistic values of the broadening (black curve). Interestingly, whereas for s states the valley-orbit splitting is negligible for the given diameter, it reaches several tens of millielectronvolts for transverse p states of both electrons and holes and can be well seen in Figure 2b.

The peaks 4 and 5 in Figure 2a correspond to the transitions between d and f states, respectively. However, contrary to the case of p states, it becomes difficult to distinguish the individual contributions of the transitions between the states with different orbital momentum projections to the absorption peaks. The band anisotropy only leads to the additional broadening of the absorption peaks. Moreover, for highly excited states, the anisotropic splitting becomes comparable to the distance between d and f multiplets so that these multiplets overlap. Hence, in what follows we will focus on the lowest transitions 1−3.

To verify our assignment of the absorption peaks, we have plotted in Figure 3 distributions of electron densities for the corresponding confined states in the reciprocal space. To this

DOI: 10.1021/acs.jpcc.7b10778
J. Phys. Chem. C 2017, 121, 27766−27773

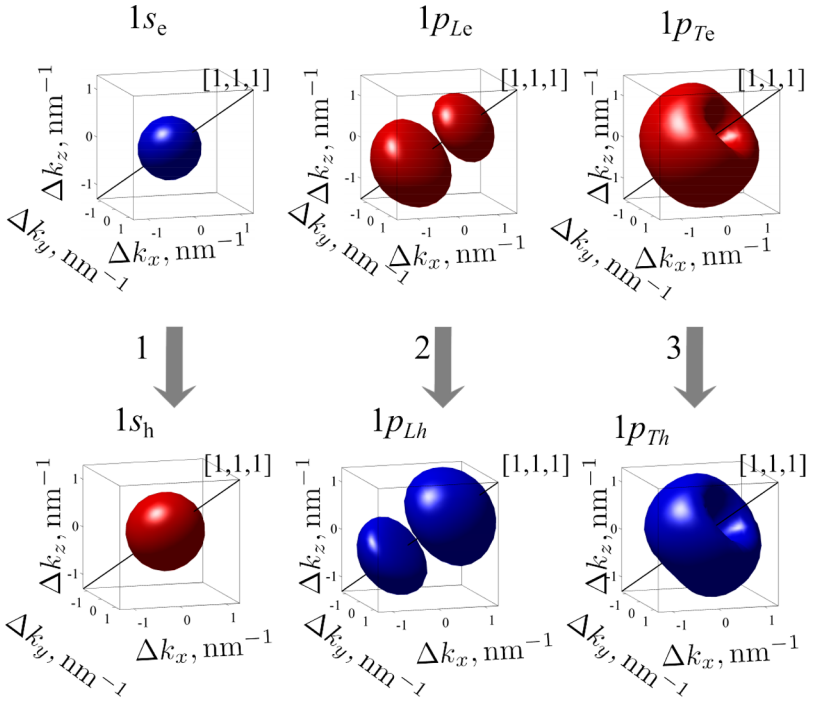

Figure 3. Reciprocal space distribution of the wave function densities corresponding to the transitions 1−3 in Figure 2. Isodensity surfaces of the *k*-space density of states summed over valley and spin degeneracy are shown.

end we have replaced the tight-binding orbitals by the δ functions, calculated the Fourier transform for each orbital, and summed the probability densities in the reciprocal space over orbital indices. Next, the probability densities were averaged over the states corresponding to different spin directions and different valleys. The calculated surfaces of constant density in the reciprocal space, shown in Figure 3, clearly visualize the symmetry of the atomistically calculated states and allow direct interpretation in terms of the $\boldsymbol{k}\cdot\boldsymbol{p}$ method. Namely, the surfaces of constant density for the s states have a close-to-spherical form. For the longitudinal p states, the surfaces consist of ellipsoids shifted along the [1, 1, 1] wave vector direction of the *L* valley. For the transverse p states, the surfaces have a shape of a doughnut oriented perpendicular to the valley direction.

Comparison of Theory and Experiment. Now we proceed to the comparison of calculated and experimental absorption spectra. Two typical spectra measured at T = 77 K are shown in Figure 4. The samples had the diameter of 10.2 nm as estimated by SAXS and the size dispersion of 5.5% (black curve) and 4% (red curve). The measured absorption spectrum well agrees with the calculated one. Namely, all transitions 1−5 are clearly resolved. Both in theoretical Figure 2 and in experimental Figure 4 the peak 2 has lower intensity and is seen as a shoulder at the low-energy side of the peak 3. This can be crudely explained by the fact that there are half as many longitudinal p states (peak 2) as there are transverse ones (peak 3), and hence the effective total oscillator strength for the p_L−p_L transition is lower. A good correspondence between the measured and calculated absorption spectra confirms our interpretation of the second and third optical transitions in PbS nanocrystals as the anisotropy-split transitions between p states[24−27] rather than the transitions between the states of different parity.[23,28−30,34]

Size Dependence of the Absorption Spectra. The raw absorption spectra, measured at T = 4 K, for samples of nanocrystals with different mean diameters, ranging from D =

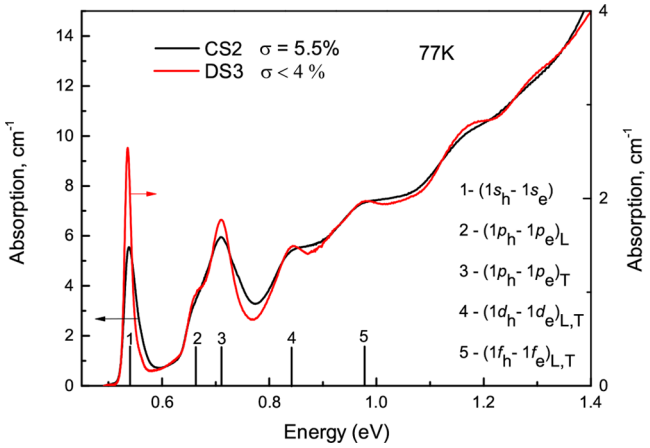

Figure 4. Absorption spectra for two samples with different size dispersion ($\delta D/D$ = 5.5% for CS2; <4% for DS3) and the same mean diameter $D \approx$ 10 nm.

5.0 to 10.2 nm are shown in Figure 5a−e. Depending on the particular sample quality, up to 7 optical transitions can be resolved. Figure 5f shows the calculated absorption spectra in the wide range of diameters D = 4.7 ÷ 10.6 nm. For diameters above 7 nm the spectral range was limited by the number of calculated confined states and the spectra are cut off at larger energies. The theoretical spectra were calculated with the homogeneous Gaussian broadening of 20 meV. The overall structure of both measured and calculated absorption spectra is the same as in Figure 4 and weakly depends on the diameters. The spectra exhibit blue shifts for smaller diameters. For small nanocrystals, $D \leq$ 7 nm, an intermediate absorption peak can be resolved in Figure 5f between the peaks 2 and 3 that corresponds to the p_L−p_T transitions between the states with different orbital momentum projections on the *L* valley axis. For each diameter, the experimental spectra were carefully

DOI: 10.1021/acs.jpcc.7b10778
J. Phys. Chem. C 2017, 121, 27766−27773

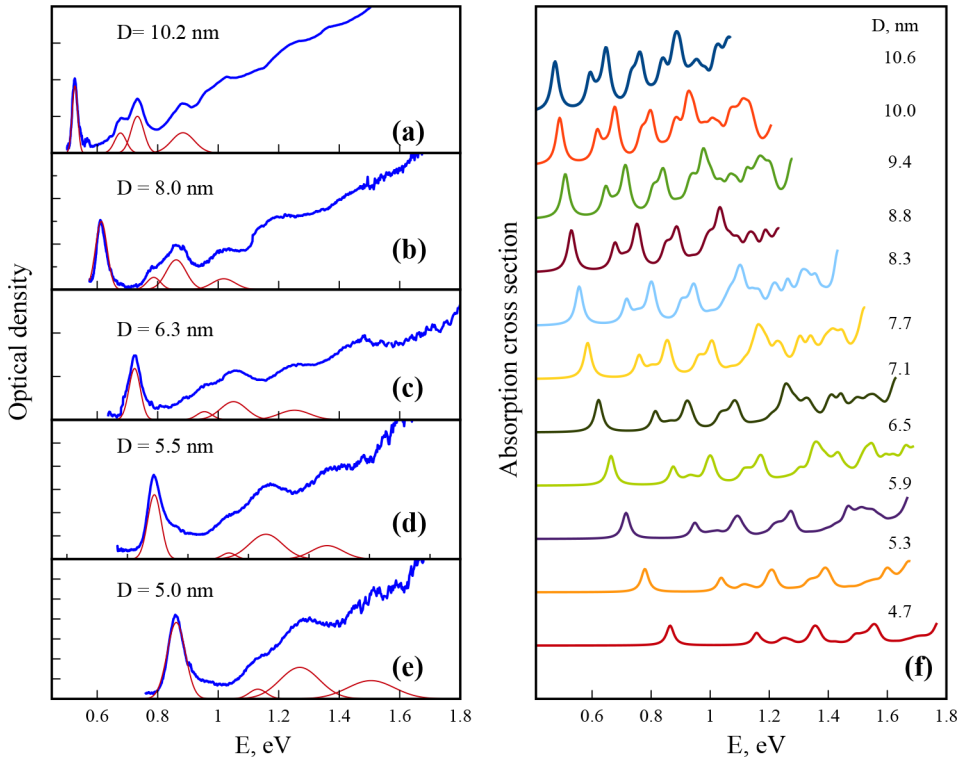

Figure 5. (a–e) Blue lines: Experimental absorption spectra of PbS quantum dots with average diameter D = 10.2, 8.0, 6.3, 5.5, and 5.0 nm, respectively, and T = 4 K. Red lines: Fits of the experimental data using the Gaussian functions. (f) Calculated photon absorption cross sections for single PbS quantum dots with diameters 4.7–10.6 nm.

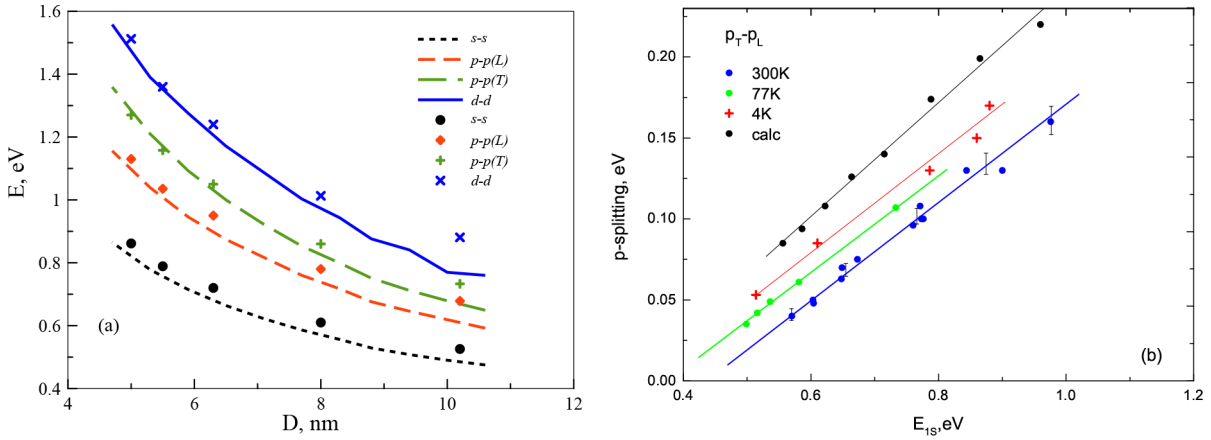

Figure 6. (a) Positions of the s–s (black dots, short dashed line), p–p(L) (red diamonds, dashed line), p–p(T) (green crosses, long dashed line), and d–d (blue x, solid line) optical transitions as functions of the quantum dot diameter obtained from the experimental data (symbols) and theoretical calculations (lines). (b) Energy splitting of the first excited state as a function of the ground-state energy of the quantum dot measured at different temperatures (blue dots: 300 K, green dots: 77 K, red crosses: 4 K) and calculated in this work (black dots).

analyzed to extract the transition energies. To this end we decomposed the spectra into the Gaussian peaks, shown in Figure 5a–e. The comparison of all obtained spectral data with our theoretical results is shown in Figure 6a that summarizes our main results. The overall behavior of the measured transition energies agrees well with our calculation. There exists a systematic blue shift of the measured peak energies as compared with the calculated ones. This blue shift is ~50 meV, and it is almost independent of the diameter or the transition energy. Two explanations are possible for the origin of the blue shift. The first one is the uncertainty in the determination of the size of nanocrystals from SAXS measurements. According to our estimations, the used procedure for extraction of the diameters from SAXS spectra can overestimate the nanocrystal diameters by about 10÷15%, which would explain the observed discrepancy. The second possible explanation is associated with the known sensitivity of the energy gap of nanocrystals to the boundary conditions used in tight-binding calculations.[45] In our work[41] we compared results of the calculations done for coated PbS nanocrystals and PbS nanocrystals with abrupt boundaries and found that boundary conditions can be responsible for the difference in nanocrystal energy gap ~50 meV. The presence of the overall spectral shift does not affect our assignment of the

DOI: 10.1021/acs.jpcc.7b10778
J. Phys. Chem. C 2017, 121, 27766–27773

second and third optical absorption peaks to the p_L-p_L and p_T-p_T transitions, respectively.

CONCLUSIONS

High-quality PbS nanocrystals in glass matrices with the mean diameters in the range of D = 4÷11 nm and size dispersion below 5% were synthesized. The mean diameters and size dispersion of the nanocrystal samples were determined by means of the small-angle X-ray scattering technique. The optical absorption spectra were measured and compared with our atomistic calculations based on the empirical tight-binding method. The calculations quantitatively account for all of the features of the PbS band structure, including the band anisotropy and the valley-orbit splittings. An analysis of the calculated transition energies, oscillator strengths, and wave function symmetry has been performed to uncover the origin of the optical transitions. Good agreement between experimental and theoretical absorption spectra has allowed us to identify the origin of lowest five absorption peaks in PbS nanocrystals and assign them to transitions between the s, p, d, and f confined states of holes and electrons with the same orbital momentum. Moreover, we have experimentally resolved the anisotropic splitting of p states with the orbital momentum oriented along and perpendicular to the L valley direction, respectively. No parity-breaking effects have been revealed either in the calculations or in the experiment. Hence, our findings strongly support the attribution of the second and third optical transitions in PbS nanocrystals to the anisotropy−split transitions between p states, rather than to the parity-breaking s−p transitions. We hope that this study will help to finally solve the long-standing controversy about the origin of the high-energy absorption peaks in spectra of lead chalcogenide nanocrystals and provide useful physical insights into their successful applications in optoelectronics and photovoltaics.

EXPERIMENTAL METHODS

Sample Preparation and SAXS Characterization. Two glasses of sodium-zinc-alumino-silicate system were used for growing PbS nanocrystals. The detailed composition of glasses can be found elsewhere.[43] The basic glass (marked CS) was synthesized by a conventional melting technique using a covered crucible to prevent volatilization of sulfur. The other glass (marked DS) was prepared by remelting the CS glass to obtain a more dilute solution of lead sulfide in the matrix. The main purpose was to avoid an early beginning of diffusion interaction between growing PbS particles during the precipitation process. As shown by Atonen et al.,[46] this interaction broadens the size distribution of nanoparticles even before the coalescence stage.[47] A theoretical consideration of these effects proposed in ref 48 qualitatively describes the results of Atonen et al.[46] Using the DS glass, we were able to obtain samples with the lowest size dispersion of PbS nanocrystals by growing them at the initial stage of the precipitation process, when the average size of nanocrystals increases proportionally to the duration of the heat treatment, $D \propto \sqrt{t}$. The absorption spectra in Figure 4 clearly demonstrate the result.

As-prepared glasses were practically uncolored, and their absorption spectra did not show any features at wavelength above 500 nm. To precipitate lead sulfide phase, glass samples were subjected to secondary heat treatments using a two-stage procedure.[49] The glass samples were annealed at 440÷450 °C (glass-transition temperature T_g is ∼485 °C) for 150 h to form PbS nuclei. The second annealing was carried out at the fixed temperature of 530÷580 °C to grow PbS nanocrystals. Both temperature and duration of the second annealing were varied to obtain nanocrystals of different sizes.

The samples containing PbS nanocrystals were examined by the small-angle X-ray scattering (SAXS) technique with the use of a laboratory setup[50,51] having a slit collimation system. The SAXS intensity was measured in 7′÷450′ scattering angle range using Ni-filtered Cu Kα radiation with the wavelength of 0.154 nm. The measurements were performed in the geometry of an "infinitely" high primary beam. In the case of scattering by identical particles of arbitrary shape the angular dependence of SAXS intensity can be approximately described by the equation

$$I(s) \approx I(0)\exp(-s^2R_g^2/3) \text{ at } sR_g \lesssim 1 \quad (1)$$

where R_g is the radius of gyration of a particle, $s = 4\pi\sin(\varphi/2)/\lambda$, φ is the scattering angle, and λ is the wavelength of X-ray radiation. The radius of gyration can be estimated from the dependence of $\ln I(s)$ on s^2, known as the Guinier plot. The size of PbS nanocrystals was determined by modeling the samples by ensembles of monodisperse spherical particles. The radius is then given by $R = (5/3)^{1/2}R_g$.

To estimate the size dispersion of nanocrystals we measured the scattered intensity in a wider range of the parameter sR. Because of low concentration of PbS nanocrystals in our samples the angular dependence of the scattered intensity can be described by the following equation

$$I(s) = I_0\int_0^\infty R^6F^2(sR)P(R)\,dR \quad (2)$$

where $F(sR) = 3\,[\sin(sR) - sR\cos(sR)]/(sR)^3$[52] and $P(R)$ is the size distribution function. We use the normal size distribution in calculations. The calculated dependencies for different values of the size dispersion are shown in Figure 7. It should be noted here that the experimental scattering curve in Figure 1a is given after the introduction of the collimation correction.

Optical Setup. Transmission spectra at liquid helium temperatures were measured using a homemade setup based on a closed-cycle helium cryostat and a prism spectrometer. The resolution of the spectrometer was 2 nm in the range of 1000 to 2500 nm and gradually increased to the visible region

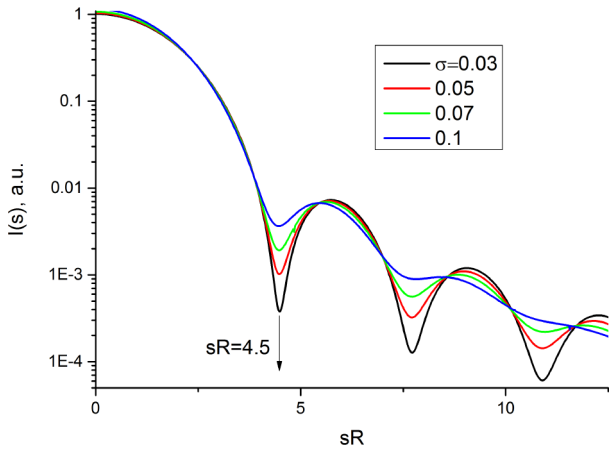

Figure 7. Calculated SAXS scattering intensity, $I(s)$, as a function of the parameter s for different values of the size dispersion, σ.

DOI: 10.1021/acs.jpcc.7b10778
J. Phys. Chem. C 2017, 121, 27766−27773

of the spectrum. The spectrometer was calibrated using optical glasses with rare-earth elements. The light from the incandescent lamp was focused on the input slit of the spectrometer set at a given wavelength. The transmitted light with a spectral width on the order of 5 nm was focused on the sample in a 1 × 5 mm strip. The power of the light incident on the sample was from 0.1 to 2 mW. After the sample, the light was focused on the surface of the bolometer with an InSb sensitive element cooled with a Pellet element to a temperature of −30 °C. To avoid simultaneous recording of the transmittance and photoluminescence, the beam transmitted through the sample was collimated by a diaphragm. The incident light was modulated with a chopper. The signal from the detector was recorded by a lock-in amplifier at a modulation frequency of 400 Hz. A closed-loop cryostat provided cooling of the sample to the temperature of 5 K. To determine the position of the levels in the transmission spectra, we fitted the spectrum with a function of the form $y(E) = A \exp[(E - E_c)/E_0] + \sum_i B_i \exp[-(E - E_i)^2/dE_i]$, where the first term describes the total exponential growth of the absorption coefficient and the sum of Gaussians expresses contributions of different transitions at E_i.

Transmission spectra at room and liquid-nitrogen temperatures were measured using Lambda 900 UV−vis−NIR spectrophotometer (PerkinElmer) with 0.2 nm resolution in the 1000−2500 nm range and a cryostat equipped with a temperature controller.

AUTHOR INFORMATION

Corresponding Authors

*R.V.C.: E-mail: r.cherbunin@spbu.ru.

*S.V.G.: E-mail: serguei.goupalov@jsums.edu.

ORCID

Roman V. Cherbunin: 0000-0002-8791-6227

Notes

The authors declare no competing financial interest.

ACKNOWLEDGMENTS

The tight-binding calculations of PbS nanocrystals were supported by the Russian Science Foundation Grant No. 14-12-01067. A.N.P. acknowledges the use of high-performance computation facilities of the ITMO University. The work of S.V.G. was supported by the National Science Foundation (NSF-CREST Grant HRD-1547754). The authors acknowledge Saint-Petersburg State University for a research grant 11.34.2.2012.

REFERENCES

(1) Bakueva, L.; Musikhin, S.; Hines, M. A.; Chang, T.-W. F.; Tzolov, M.; Scholes, G. D.; Sargent, E. H. Size-Tunable Infrared (1000 − 1600 nm) Electroluminescence from PbS Quantum-Dot Nanocrystals in a Semiconducting Polymer. *Appl. Phys. Lett.* **2003**, *82*, 2895−2897.

(2) Bakueva, L.; Konstantatos, G.; Levina, L.; Musikhin, S.; Sargent, E. H. Luminescence from Processible Quantum Dot-Polymer Light Emitters 1100-1600 nm: Tailoring Spectral Width and Shape. *Appl. Phys. Lett.* **2004**, *84*, 3459−3461.

(3) Supran, G. J.; Song, K. W.; Hwang, G. W.; Correa, R. E.; Scherer, J.; Dauler, E. A.; Shirasaki, Y.; Bawendi, M. G.; Bulović, V. High-Performance Shortwave-Infrared Light-Emitting Devices Using Core-Shell (PbS-CdS) Colloidal Quantum Dots. *Adv. Mater.* **2015**, *27*, 1437−1442.

(4) Gong, X.; Yang, Z.; Walters, G.; Comin, R.; Ning, Z.; Beauregard, E.; Adinolfi, V.; Voznyy, O.; Sargent, E. H. Highly Efficient Quantum Dot Near-Infrared Light-Emitting Diodes. *Nat. Photonics* **2016**, *10*, 253−257.

(5) McDonald, S. A.; Konstantatos, G.; Zhang, S.; Cyr, P. W.; Klem, E. J. D.; Levina, L.; Sargent, E. H. Solution-Processed PbS Quantum Dot Infrared Photodetectors and Photovoltaics. *Nat. Mater.* **2005**, *4*, 138−142.

(6) Saran, R.; Curry, R. J. Lead Sulphide Nanocrystal Photodetector Technologies. *Nat. Photonics* **2016**, *10*, 81−92.

(7) Ellingson, R. J.; Beard, M. C.; Johnson, J. C.; Yu, P.; Micic, O. I.; Nozik, A. J.; Shabaev, A.; Efros, A. L. Highly Efficient Multiple Exciton Generation in Colloidal PbSe and PbS Quantum Dots. *Nano Lett.* **2005**, *5*, 865−871.

(8) Nozik, A. J.; Beard, M. C.; Luther, J. M.; Law, M.; Ellingson, R. J.; Johnson, J. C. Semiconductor Quantum Dots and Quantum Dot Arrays and Applications of Multiple Exciton Generation to Third-Generation Photovoltaic Solar Cells. *Chem. Rev.* **2010**, *110*, 6873−6890.

(9) Carey, G. H.; Abdelhady, A. L.; Ning, Z.; Thon, S. M.; Bakr, O. M.; Sargent, E. H. Colloidal Quantum Dot Solar Cells. *Chem. Rev.* **2015**, *115*, 12732−12763.

(10) Wu, M.; Congreve, D. N.; Wilson, M. W. B.; Jean, J.; Geva, N.; Welborn, M.; Van Voorhis, T.; Bulović, V.; Bawendi, M. G.; Baldo, M. A. Solid-State Infrared-to-Visible Upconversion Sensitized by Colloidal Nanocrystals. *Nat. Photonics* **2015**, *10*, 31−34.

(11) Cao, Y.; Stavrinadis, A.; Lasanta, T.; So, D.; Konstantatos, G. The Role of Surface Passivation for Efficient and Photostable PbS Quantum Dot Solar Cells. *Nat. Energy* **2016**, *1*, 16035.

(12) Hines, M.; Scholes, G. Colloidal PbS Nanocrystals with Size-Tunable Near-Infrared Emission: Observation of Post-Synthesis Self-Narrowing of the Particle Size Distribution. *Adv. Mater.* **2003**, *15*, 1844−1849.

(13) Cademartiri, L.; Montanari, E.; Calestani, G.; Migliori, A.; Guagliardi, A.; Ozin, G. A. Size-Dependent Extinction Coefficients of PbS Quantum Dots. *J. Am. Chem. Soc.* **2006**, *128*, 10337−10346.

(14) Moreels, I.; Lambert, K.; Smeets, D.; De Muynck, D.; Nollet, T.; Martins, J. C.; Vanhaecke, F.; Vantomme, A.; Delerue, C.; Allan, G.; et al. Size-Dependent Optical Properties of Colloidal PbS Quantum Dots. *ACS Nano* **2009**, *3*, 3023−3030.

(15) Weidman, M. C.; Beck, M. E.; Hoffman, R. S.; Prins, F.; Tisdale, W. A. Monodisperse, Air-Stable PbS Nanocrystals via Precursor Stoichiometry Control. *ACS Nano* **2014**, *8*, 6363−6371.

(16) Moreels, I.; Justo, Y.; De Geyter, B.; Haustraete, K.; Martins, J. C.; Hens, Z. Size-Tunable, Bright, and Stable PbS Quantum Dots: A Surface Chemistry Study. *ACS Nano* **2011**, *5*, 2004−2012.

(17) Zherebetskyy, D.; Scheele, M.; Zhang, Y.; Bronstein, N.; Thompson, C.; Britt, D.; Salmeron, M.; Alivisatos, P.; Wang, L.-W. Hydroxylation of the Surface of PbS Nanocrystals Passivated with Oleic Acid. *Science* **2014**, *344*, 1380−1384.

(18) Bertolotti, F.; Dirin, D. N.; Ibáñez, M.; Krumeich, F.; Cervellino, A.; Frison, R.; Voznyy, O.; Sargent, E. H.; Kovalenko, M. V.; Guagliardi, A.; et al. Crystal Symmetry Breaking and Vacancies in Colloidal Lead Chalcogenide Quantum Dots. *Nat. Mater.* **2016**, *15*, 987−994.

(19) Weidman, M. C.; Smilgies, D.-M.; Tisdale, W. A. Kinetics of the Self-Assembly of Nanocrystal Superlattices Measured by Real-Time in situ X-ray Scattering. *Nat. Mater.* **2016**, *15*, 775−781.

(20) Lin, P. J.; Kleinman, L. Energy Bands of PbTe, PbSe, and PbS. *Phys. Rev.* **1966**, *142*, 478−489.

(21) Kang, I.; Wise, F. W. Electronic Structure and Optical Properties of PbS and PbSe Quantum Dots. *J. Opt. Soc. Am. B* **1997**, *14*, 1632−1646.

(22) Preier, H. Recent Advances in Lead-Chalcogenide Diode Lasers. *Appl. Phys.* **1979**, *20*, 189−206.

(23) Harbold, J. M.; Du, H.; Krauss, T. D.; Cho, K.-S.; Murray, C. B.; Wise, F. W. Time-Resolved Intraband Relaxation of Strongly Confined Electrons and Holes in Colloidal PbSe Nanocrystals. *Phys. Rev. B: Condens. Matter Mater. Phys.* **2005**, *72*, 195312.

DOI: 10.1021/acs.jpcc.7b10778
J. Phys. Chem. C 2017, 121, 27766−27773

(24) Andreev, A. D.; Lipovskii, A. A. Anisotropy-Induced Optical Transitions in PbSe and PbS Spherical Quantum Dots. *Phys. Rev. B: Condens. Matter Mater. Phys.* **1999**, *59*, 15402−15404.
(25) Andreev, A. D.; Kolobkova, E. V.; Lipovskii, A. A. Optical Absorption in PbSe Spherical Quantum Dots Embedded in Glass Matrix. *J. Appl. Phys.* **2000**, *88*, 750−757.
(26) Bartnik, A. C.; Efros, A. L.; Koh, W.-K.; Murray, C. B.; Wise, F. W. Electronic States and Optical Properties of PbSe Nanorods and Nanowires. *Phys. Rev. B: Condens. Matter Mater. Phys.* **2010**, *82*, 195313.
(27) An, J. M.; Franceschetti, A.; Dudiy, S. V.; Zunger, A. The Peculiar Electronic Structure of PbSe Quantum Dots. *Nano Lett.* **2006**, *6*, 2728−2735.
(28) Allan, G.; Delerue, C. Confinement Effects in PbSe Quantum Wells and Nanocrystals. *Phys. Rev. B: Condens. Matter Mater. Phys.* **2004**, *70*, 245321.
(29) Peterson, J. J.; Huang, L.; Delerue, C.; Allan, G.; Krauss, T. D. Uncovering Forbidden Optical Transitions in PbSe Nanocrystals. *Nano Lett.* **2007**, *7*, 3827−3831.
(30) Goupalov, S. V. Selection Rules for Optical Transitions in PbSe Nanocrystal Quantum Dots: Drastic Effect of Structure Inversion Asymmetry. *Phys. Rev. B: Condens. Matter Mater. Phys.* **2009**, *79*, 233305.
(31) Trinh, M. T.; Houtepen, A. J.; Schins, J. M.; Piris, J.; Siebbeles, L. D. A. Nature of the Second Optical Transition in PbSe Nanocrystals. *Nano Lett.* **2008**, *8*, 2112−2117.
(32) Liljeroth, P.; van Emmichoven, P. A. Z.; Hickey, S. G.; Weller, H.; Grandidier, B.; Allan, G.; Vanmaekelbergh, D. Density of States Measured by Scanning-Tunneling Spectroscopy Sheds New Light on the Optical Transitions in PbSe Nanocrystals. *Phys. Rev. Lett.* **2005**, *95*, 086801.
(33) Nootz, G.; Padilha, L. A.; Olszak, P. D.; Webster, S.; Hagan, D. J.; Van Stryland, E. W.; Levina, L.; Sukhovatkin, V.; Brzozowski, L.; Sargent, E. H. Role of Symmetry Breaking on the Optical Transitions in Lead-Salt Quantum Dots. *Nano Lett.* **2010**, *10*, 3577−3582.
(34) Diaconescu, B.; Padilha, L. A.; Nagpal, P.; Swartzentruber, B. S.; Klimov, V. I. Measurement of Electronic States of PbS Nanocrystal Quantum Dots Using Scanning Tunneling Spectroscopy: The Role of Parity Selection Rules in Optical Absorption. *Phys. Rev. Lett.* **2013**, *110*, 127406.
(35) Su, G.; Liu, C.; Deng, Z.; Zhao, X.; Zhou, X. Size-dependent Photoluminescence of PbS QDs Embedded in Silicate Glasses. *Opt. Mater. Express* **2017**, *7*, 2194−2207.
(36) Joshi, S.; Sen, S.; Ocampo, P. Nucleation and Growth Kinetics of PbS Quantum Dots in Oxide Glass: Spectroscopic and Microscopic Studies in the Dilute Range. *J. Phys. Chem. C* **2007**, *111*, 4105−4110.
(37) Lipovskii, A.; Kolobkova, E.; Olkhovets, A.; Petrikov, V.; Wise, F. Synthesis of Monodisperse PbS Quantum Dots in Phosphate Glass. *Phys. E* **1999**, *5*, 157−160.
(38) Hummer, K.; Grüneis, A.; Kresse, G. Structural and Electronic Properties of Lead Chalcogenides from First Principles. *Phys. Rev. B: Condens. Matter Mater. Phys.* **2007**, *75*, 195211.
(39) Svane, A.; Christensen, N. E.; Cardona, M.; Chantis, A. N.; van Schilfgaarde, M.; Kotani, T. Quasiparticle Self-Consistent GW Calculations for PbS, PbSe, and PbTe: Band Structure and Pressure Coefficients. *Phys. Rev. B: Condens. Matter Mater. Phys.* **2010**, *81*, 245120.
(40) Laflamme Janssen, J.; Gillet, Y.; Poncé, S.; Martin, A.; Torrent, M.; Gonze, X. Precise Effective Masses from Density Functional Perturbation Theory. *Phys. Rev. B: Condens. Matter Mater. Phys.* **2016**, *93*, 205147.
(41) Poddubny, A. N.; Nestoklon, M. O.; Goupalov, S. V. Anomalous Suppression of Valley Splittings in Lead Salt Nanocrystals without Inversion Center. *Phys. Rev. B: Condens. Matter Mater. Phys.* **2012**, *86*, 035324.
(42) Ekimov, A.; Efros, A.; Onushchenko, A. Quantum Size Effect in Semiconductor Microcrystals. *Solid State Commun.* **1985**, *56*, 921−924.
(43) Shepilov, M.; Anan'ev, A.; Maksimov, L.; Savostyanov, V.; Golubkov, V.; Onushchenko, P.; Ananyev, V.; Onushchenko, A. Landau-Placzek Ratio of an Inorganic Glass with PbS Quantum Dots. *J. Non-Cryst. Solids* **2016**, *450*, 156−163.
(44) Goupalov, S. V.; Ivchenko, E. L. A Tight-Binding Representation of Electron-Hole Exchange Interaction in Semiconductors. *Phys. Solid State* **2001**, *43*, 1867−1875.
(45) Delerue, C.; Lannoo, M.; Allan, G. Comment on "Size Dependence of Excitons in Silicon Nanocrystals. *Phys. Rev. Lett.* **1996**, *76*, 3038.
(46) Atonen, O. V.; Golubkov, V. V.; Onushchenko, A. A. Influence of Heat Treatment Conditions on the Precipitation and Dissolution of Lead Sulfide Nanocrystals in Sodium Zinc Silicate Glasses. *Glass Phys. Chem.* **2010**, *36*, 389−397.
(47) Lifshitz, I.; Slezov, V. Kinetics of Diffusive Decomposition of Supersaturated Solid Solutions. *Sov. Phys. JETP* **1959**, *35*, 331−339.
(48) Shepilov, M. Calculation of Kinetics of Metastable Liquid-liquid Phase Separation for the Model with Simultaneous Nucleation of Particles. *J. Non-Cryst. Solids* **1992**, *146*, 1−25.
(49) Alekseeva, I. P.; Atonen, O. V.; Golubkov, V. V.; Onushchenko, A. A.; Raaben, E. L. Kinetic Regularities of the Precipitation of PbS Nanocrystals in Sodium Zinc Silicate Glasses. *Glass Phys. Chem.* **2007**, *33*, 1−7.
(50) Golubkov, V.; Vasilevskaya, T.; Porai-Koshits, E. SAXS Study of the Structure of Glasses Containing no Modifying Oxides. *J. Non-Cryst. Solids* **1980**, *38*−*39*, 99−104.
(51) Golubkov, V.; Titov, A.; Porai-Koshits, E. SAXS Apparatus for a Study of Glasses at High Temperatures. *Pribory i Tekhnika Experimen. (in Russian)* **1975**, *1*, 215−217.
(52) Guinier, A.; Fournet, G. *Small-Angle Scattering of X-rays*; John Wiley & Sons Inc.: New York, 1955.

DOI: 10.1021/acs.jpcc.7b10778
J. Phys. Chem. C 2017, 121, 27766−27773